24th NATIONAL RADIO SCIENCE CONFERENCE (NRSC 2007)
March 13-15, 2007
Faculty of Engineering, Ain shams Univ., Egypt

Analysis of Different Fiber Bragg Gratings for Use in a Multi-wavelength Erbium Doped Fiber Laser

Mohamed M. Keshk[#] (mohk444@hotmail.com),
Islam A. Ashry[#](eng_islam_ashry@yahoo.com)
Moustafa H. Aly[*](mosaly@aast.edu), Ali M. Okaz[#](Ali_okaz@yahoo.com)

Faculty of Engineering, University of Alexandria, Alexandria, Egypt.
* College of Engineering and Technology, Arab Academy for Science & Technology & Maritime Transport, Alexandria, Egypt and Member of OSA.

Abstract
A simple multi-wavelength laser source using, an erbium doped fiber (EDF) as a gain medium is proposed. The source is terminated by a chirped fiber Bragg grating (CFBG) on one side and cascaded FBGs on the other side. Different apodization profiles for the FBG are analyzed to improve the lasing wavelengths selectivity. The Blackman profile is found to be the best to reduce the reflection spectrum sidelobes with a maximum reflectivity of 99%.

Keywords: Apodization, Fiber Bragg grating (FBG), Erbium doped fiber laser (EDFL).

1. Introduction
Multi-wavelength fiber lasers are of great interest for applications such as wavelength division multiplexing (WDM) fiber communication systems, fiber sensors and optical instrument testing. Various techniques have been proposed to realize multi- wavelength oscillations in erbium doped fiber lasers (EDFLs) [1-4].

Fiber Bragg gratings (FBGs) are ideal wavelength selection components for fiber lasers due to the unique advantages such as fiber compatibility, ease of use and low cost. Different types of FBGs and different topologies have been used in order to perform simple or more elaborate filtering functions. These include cascaded fiber Bragg grating [3], a FBG written in a high birefringent fiber [2], and sampled FBG [4]. The main peak in the reflection spectrum of a finite length Bragg grating with uniform modulation of the index of refraction is accompanied by a series of sidelobes at adjacent wavelengths. It is important in some applications to lower and, if possible, eliminate the reflectivity of these sidelobes, or to apodize the reflection spectrum of the grating [5].

In this paper, many types of apodization profiles are investigated to improve the characteristics of simple multi-wavelength EDF laser using a chirped fiber Bragg grating (CFBG) and cascaded uniform fiber Bragg gratings.

2. Theory
The relation between the spectral dependence of a fiber grating and the corresponding grating structure is usually described by the coupled-mode theory [5-7]. The grating is treated as a perturbation on the fiber. The unperturbed fiber has refractive index profile $\bar{n}(x, y)$ and the perturbed fiber has the z-dependent index n(x, y, z). Perturbed and unperturbed fibers are weakly guiding. So, one can assume $\bar{n} \cong n \cong n_{eff} \cong n_{cl}$, where n_{cl} is the cladding index and n_{eff} is the effective index of the modes in the absence of the grating. For a fiber grating, the z-dependence of the index perturbation is approximately quasi-sinusoidal in the sense that it can be written as

$$n = \bar{n} + \Delta n(z)\cos\left(\frac{2\pi}{\Lambda}z + \theta(z)\right), \tag{1}$$

where Λ is a chosen design period so that $\theta(z)$ becomes a slowly varying function of z compared to the period Λ. The function $\Delta n(z)$ is real and slowly varying called the amplitude of index modulation. Along the grating, the forward and backward propagating waves, u(z) and v(z), are related by the coupled mode equations

$$\frac{du}{dz} = +i\delta u + \mathbf{k}(z)v,$$

$$\frac{dv}{dz} = -i\delta v + \mathbf{k}^{*}(z)u, \tag{2}$$

where the amplitudes, u(z) and v(z), of the waves u and v are related to the amplitudes of the forward and backward propagating electric fields, b_1 and b_{-1}, respectively, by

$$b_1(z) = u(z)\exp\left(+i\frac{\pi}{\Lambda}z\right),$$

$$b_{-1}(z) = v(z)\exp\left(-i\frac{\pi}{\Lambda}z\right), \tag{3}$$

with $\mathbf{k}(z)$, the coupling coefficient given by

$$k(z) = k^*(z) = \frac{\eta\pi\Delta n(z)}{\lambda_B}, \tag{4}$$

$$\arg\mathbf{k}(z) = \theta(z) + \frac{\pi}{2}, \tag{5}$$

and δ ($= n_{eff}\,\omega / c - \pi / \Lambda$) represents the detuning from the Bragg grating resonance wavelength λ_B ($= 2n_{eff}\,\Lambda$).
In the uniform gratings $k(z) = k$ = constant because $\Delta n(z) = \Delta n$ = constant and $\theta(z) = 0$. In this situation, the coupled-mode equations can be solved analytically to give a reflection coefficient of the form

$$\mathbf{r}(L,\lambda) = \frac{-\mathbf{k}^*\sinh(sL)}{s\cosh(sL) - i\delta\sinh(sL)}, \tag{6}$$

with $s^2 = k^2 - \delta^2$.
The transmission coefficient, t (L, λ) becomes

$$\mathbf{t}(L,\lambda) = \frac{s}{s\cosh(sL) - i\delta\sinh(sL)}. \tag{7}$$

Easily, one can find expressions for the reflectivity and transmissivity T(L,λ) as follows

$$R(L,\lambda) = \frac{k^2\sinh^2(sL)}{s^2\cosh^2(sL) + \delta^2\sinh^2(sL)}. \tag{8}$$

$$T(L,\lambda) = \frac{s^2}{s^2\cosh^2(sL) + \delta^2\sinh^2(sL)}. \tag{9}$$

There is a variety of methods to compute the reflection and transmission spectra for nonuniform (chirped and apodized) gratings [5, 6]. Here, the most extensively used method called transfer matrix method is presented. The grating is divided into a sufficient number N of sections so that each section can be approximately treated as uniform. Let the section length be $\Delta = L / N$. Solving the coupled-mode equations, one gets the transfer matrix relation between the fields at z and at $z + \Delta$ as

$$\begin{bmatrix} u(z+\Delta) \\ v(z+\Delta) \end{bmatrix} = M_T \begin{bmatrix} u(z) \\ v(z) \end{bmatrix}, \tag{10}$$

where

$$M_T = \begin{bmatrix} \cosh(s\Delta) + i\sinh(s\Delta) & \frac{\mathbf{k}}{s}\sinh(s\Delta) \\ \frac{\mathbf{k}^*}{s}\sinh(s\Delta) & \cosh(s\Delta) - i\frac{\delta}{s}\sinh(s\Delta) \end{bmatrix}$$

Hence, one can connect the fields at the two ends of the grating through

$$\begin{bmatrix} u(L) \\ v(L) \end{bmatrix} = T \begin{bmatrix} u(0) \\ v(0) \end{bmatrix}, \tag{11}$$

where $T = T_N.T_{N-1}\ldots T_i\ldots T_1$ is the overall transfer matrix and T_i is the transfer matrix written in Eq.10 with $\mathbf{k} = \mathbf{k}_i = \mathbf{k}(j\Delta)$ the coupling coefficient of the j^{th} section. As a result, T is a 2×2 matrix of the form

$$T = \begin{bmatrix} T_{11} & T_{12} \\ T_{21} & T_{22} \end{bmatrix}, \tag{12}$$

Once the matrix T is determined, the reflection and transmission coefficients are calculated by the relations

$$\mathbf{r}(L,\lambda) = \frac{-T_{21}}{T_{22}}.$$

$$\mathbf{t}(L,\lambda) = \frac{1}{T_{22}}. \quad (13)$$

3. Results and Discussion

The proposed system is illustrated in Fig. 1. The cascaded FBGs act as full-reflecting mirrors and wavelength selectors at different Bragg wavelengths while the CFBG acts as a broadband partially reflecting mirror with an average reflectivity = -3 dB over 13 nm band centered about 1550 nm. The EDF is 20 m long cooled in liquid nitrogen (77 K) to enable stable lasing at multiple wavelengths and pumped by a laser diode at 980 nm [4].

Using the mentioned transfer matrix method, one can get the reflectivity of the CFBG, Fig. 2. Each sub-section has a different pitch and increases linearly from z = 0 to z = L. The analysis of the CFBG is based on the following characteristics [5, 8, 9]:

1- Length = L = 5 cm.
2- Average reflectivity = -3 dB over 13 nm band centered about 1550 nm.
3- Centered wavelength = λ_c = 1550 nm.
4- Chirped value = 3 nm/cm.
5- Amplitude of index modulation = $\Delta n = 3.1 \times 10^{-4}$.
6- Core diameter = 10 μm with NA = 0.133.
7- Number of sub-sections = N = 100.
8- Effective refractive index = n_{eff} = 1.48.

Using the described model of uniform grating, the reflectivity of the cascaded FBFs are obtained and displayed in Fig. 3. Similar to the CFBG, the analysis of the cascaded uniform Bragg gratings is based on the following characteristics [5, 8, 9]:

1- Length = L = 8 mm.
2- Maximum reflectivity = $R_{max} \geq 99$ %.
3- Centered wavelengths of the cascaded FBGs = λ_B = 1544, 1547, 1550, 1553, 1556 nm.
4- Amplitude of index modulation = $\Delta n = 0.3 \times 10^{-3}$.
5- Core diameter = 10 μm with NA = 0.133.
6- Effective refractive index = n_{eff} = 1.48.

From Fig. 3, one observes that, there is a high reflectivity to the sidelobes and a 3 nm guard band between two successive Bragg wavelengths of the cascaded FBGs. This is designed to minimize the interference and accumulation of the sidelobes. High reflectivity, interference and accumulation of sidelobes may badly affect the laser output. To increase the number of lasing wavelengths and the wavelength selectivity, it is required to increase the number of cascaded FBGs. This can be achieved by the decrease of the guard band but under condition of reduction of these sidelobes by apodization as will be seen later.

The sidelobes peaks are caused as follows:

1. The refractive index of the grating section n is higher than of the fiber core $\bar{n}$ at either ends, Eq. (1), Fig. 4.
2. Light at wavelengths that are unaffected by the grating itself nevertheless "sees" an abrupt change in the refractive index at either end of the grating.
3. Thus, two partial mirrors are formed at each end of the grating.
4. These mirrors act as a Fabry-Perot interferometer and create resonance conditions between them.

These sidelobes may be removed by apodizing the grating. Apodization is a process of tapering the strength of the grating at either end so that the apparent refractive index change is gradual rather than abrupt such that $\Delta n(z)$, Eq.(1), is a slowly varying function with z, Fig. 5.

The main apodization profiles, considered in the present investigation, are [10, 11]

1. Raised sine profile

$$\Delta n(z) = \Delta n\left[\sin^2\left(\frac{\pi z}{L}\right)\right], \; 0 \leq z \leq L. \quad (14)$$

2. sine profile

$$\Delta n(z) = \Delta n\left[\sin\left(\frac{\pi z}{L}\right)\right], 0 \le z \le L. \quad (15)$$

3. sinc profile

$$\Delta n(z) = \Delta n\left[\frac{\sin(x)}{x}\right],$$

with

$$x = \frac{2\pi\left(z - \frac{L}{2}\right)}{L},\ 0 \le z \le L. \quad (16)$$

4. Gaussian profile

$$\Delta n(z) = \Delta n\left[-5\left(\frac{(z - \frac{L}{2})}{L}\right)^2\right], 0 \le z \le L. \quad (17)$$

5. Hamming profile

$$\Delta n(z) = \Delta n\left[\frac{1 + H\cos\left(\frac{2\pi(z - \frac{L}{2})}{L}\right)}{1 + H}\right],$$

$$H = 0.9,\ 0 \le z \le L. \quad (18)$$

6. tanh profile

$$\Delta n(z) = \Delta n\left[\tanh\left(\frac{8z}{L}\right)\right],\ 0 \le z \le \frac{L}{2},$$

$$= \Delta n\left[\tanh\left(\frac{8(L - z)}{L}\right)\right],\ \frac{L}{2} \le z \le L. \quad (19)$$

7. Bartlett profile

$$\Delta n(z) = \Delta n\left[\frac{2z}{L}\right],\ 0 \le z \le \frac{L}{2},$$

$$= \Delta n\left[-2\left(\frac{z}{L} - 1\right)\right],\ \frac{L}{2} \le z \le L. \quad (20)$$

8. Blackman profile

$$\Delta n(z) = \Delta n\left[\frac{1 + 1.19\cos(x) + 0.19\cos(2x)}{2.38}\right],$$

$$x = \frac{2\pi\left(z - \frac{L}{2}\right)}{L},\ 0 \le z \le L\ . \tag{21}$$

9. Cauchy profile

$$\Delta n(z) = \Delta n \left[\frac{1 - \left(\frac{2(z - \frac{L}{2})}{L} \right)^2}{1 - \left(\frac{2C(z - \frac{L}{2})}{L} \right)^2} \right],$$

$$C = 0.5,\ 0 \le z \le L\ . \tag{22}$$

For visualization and comparison, the various apodization profiles are plotted in Fig. 6.

The reflectivity of the apodized FBG is determined by considering each sub-section to have a different coupling coefficient $k(z)$ and all of them have a similar pitch.
It is noted that, for different apodization profiles, there is a reduction in the maximum reflectivity, Fig. 7, and a reduction in sidelobes, Fig. 8 on a normal and logarithmic scales respectively.

The previous results for all apodization profiles are summarized in Table 1, from which one can note that, the Blackman profile has the minimum sidelobes reduction compared to uniform FBG.

Table 1 Comparison of different profiles.

Apodization profile	Maximum reflectivity	Reduction in main sidelobes levels (dB)
Raised sine	92.55 %	38
sine	97.4 %	17
sinc	96.25 %	21
Gaussian	98.44 %	11
Hamming	93.9 %	34
tanh	99.41 %	7
Bartlett	92.55 %	14
Blackman	86.47 %	49
Cauchy	98.47 %	12

This is because the Blackman profile has nearly zero slope and no change in the refractive index than the core value at the FBG ends (z = 0 and z = L) and has the best gradual change of the refractive index elsewhere.

To discuss the second phenomenon of the reduction of maximum reflectivity, we have to analyze the behavior of reflectivity with the grating strength kL.
The reflectivity versus wavelength for different values of the grating strength, kL, is shown in Fig. 9 and the maximum reflectivity at $\lambda = \lambda_B$ is displayed against kL in Fig. 10. It is clear that, the maximum reflectivity (which is less than 100%) is proportional to (kL) for the uniform FBG and to $\int_0^L k(z)dz$ for the apodized FBG, i.e. to the area under the curve of Fig. 6 because $k(z)$ is proportional to $\Delta n(z)$, Eq. (4). As a result, the Blackman profile has the maximum reduction of maximum reflectivity because it has a minimum area under the curve. Also, the tanh profile has the minimum reduction of the maximum reflectivity because it has the maximum area under the curve or the maximum strength.

Recall to the main problem, one has to select the best apodization profile for the cascaded uniform FBG to act as a full reflecting mirror in the EDFL with minimum sidelobes to decrease the guard band and increase the number of lasing wavelengths. The maximum sidelobes reduction is obtained by Blackman profile but, it has the disadvantage of relatively low value of the maximum reflectivity (86.47%). So, the main function of the cascaded FBG as a full reflecting mirror with $R \geq 99\%$, may be lost.

An important result is indicated from Fig. 10, where the maximum reflectivity depends on the value of kL for the uniform FBG or on $\int_0^L k(z)dz$ for the apodized FBG. Define $(kL)_{cutoff}$ as the FBG strength corresponding to a maximum reflectivity of 99%. If $\int_0^L k(z)dz$ for the apodized FBG is equal to $(kL)_{cutoff}$, a FBG with a reflectivity of 99% will be obtained with a sidelobes reduction. This can be achieved by three methods:

A-Increasing the length of the apodized FBG

One can increase the strength of the apodized FBG such that

$$\int_0^{L_N} k_N(z)dz = (kL)_{cutoff}, \tag{23}$$

where, L_N and $k_N(z)$ are the new length of the increased length apodized FBG and the new coupling coefficient, respectively . The value of $(kL)_{cutoff}$ can be easily evaluated from Eq.(8) at maximum reflectivity of 99% and $\lambda = \lambda_B$ and is found = 3. To evaluate L_N, we consider the Blackman profile as a sample. The same procedure is applied to other profiles except the tanh profile because its reflectivity is already above 99%. The term $\Delta n(z)$, Eq. (21) is substituted in Eq. (4) when $L = L_N$,

$$k_N(z) = \frac{\eta\pi\Delta n_N(z)}{\lambda_B},$$

$$= \frac{\eta\pi}{\lambda_B}\left[\Delta n\left(\frac{1+1.19\cos(x)+0.19\cos(2x)}{2.38}\right)\right], \text{ with}$$

$$x = \frac{2\pi\left(z-\frac{L_N}{2}\right)}{L_N}, \tag{24}$$

Using Eq. (24) in Eq. (23), one gets

$$\int_0^{L_N} \frac{\eta\pi}{\lambda_B}\left[\Delta n\left(\frac{1+1.19\cos(x)+0.19\cos(2x)}{2.38}\right)\right]dz = (kL)_{cutoff} = 3, \text{ with}$$

$$x = \frac{2\pi\left(z-\frac{L_N}{2}\right)}{L_N}. \tag{25}$$

Equation (25) is solved resulting in $L_N = 14.48$ mm.
Similarly, Eq. (23) is solved for the other apodization profiles and the results are summarized in Table 2.

Table 2 Comparison of different profiles.

Apodization profile	L_N (mm)
Raised sine	12.17
Sine	9.56
Sinc	10.32
Gaussian	8.66
Hamming	11.56
Tanh	7.36
Barttlet	12.17
Blackman	14.48
Cauchy	8.64

As expected, all new lengths are longer than 8 mm except the tanh profile because its reflectivity is already above 99%. We will concern the Blackman profile because from Tables 1 and 2, it has a maximum sidelobes reduction but its new length, L_N, is also a maximum for a reflectivity of 99%. The length is not a main problem because there are FBGs with lengths more than 100 mm [11]. Figures 11 and 12 show the characteristics of the Blackman apodized FBG reflectivity for $\Delta n = 10^{-3}$ = constant.

Figure 11 shows an increase in the maximum reflectivity. A bonus advantage is noticed in Fig. 12 that shows an increase in the reduction of the sidelobes. This is explained as follows: for a length of 8 mm, $\Delta n(z)$ will vary from zero at z = 0 to Δn at z = (8 mm/2) = 4 mm while, for L_N = 14.48 mm, $\Delta n(z)$ will vary from zero at z = 0 to Δn at z = (14.48 mm/2) = 7.24 mm. Therefore, the gradual change of $\Delta n(z)$ is better for the new length, Fig. 13.

B – Increasing the index modulation maximum amplitude of the apodized FBG

One can increase the strength of the apodized FBG such that,

$$\int_0^L k_N(z)dz = (kL)_{cutoff}, \tag{26}$$

$$k_N(z) = \frac{\eta\pi\Delta n_N(z)}{\lambda_B}, \tag{27}$$

where, $\Delta n_N(z)$ is the new index modulation amplitude.
Concerning the Blackman profile and substituting Eq. (27) into Eq. (26) using Eq. (21), one can get

$$\int_0^L \frac{\eta\pi}{\lambda_B}\left[\Delta n_N\left(\frac{1+1.19\cos(x)+0.19\cos(2x)}{2.38}\right)\right]dz = (kL)_{cutoff} = 3,$$

with

$$x = \frac{2\pi\left(z-\frac{L}{2}\right)}{L}, \tag{28}$$

where, Δn_N is the new maximum amplitude of index modulation.
Equation (28) is solved giving $\Delta n_N = 0.543\times10^{-3}$. Similarly, Eq. (26) is solved for the other profiles and the obtained results are summarized in Table 3.

Table 3 Comparison of different apodization profiles.

Apodization profile	New maximum amplitude of index modulation Δn_N
Raised sine	0.456×10^{-3}
Sine	0.358×10^{-3}
Sinc	0.387×10^{-3}
Gaussian	0.325×10^{-3}
Hamming	0.433×10^{-3}
Tanh	0.276×10^{-3}
Barttlet	0.456×10^{-3}
Blackman	0.543×10^{-3}
Cauchy	0.324×10^{-3}

All new maximum amplitudes of index modulation are longer than 0.3×10^{-3}except the tanh profile because its reflectivity is already above 99%. From Tables 1 and 3, one concludes that, the Blackman apodization profile has a maximum sidelobes reduction, but its new maximum amplitude of index modulation Δn_N is also a maximum for reflectivity of 99%. The increase of the maximum amplitude of index modulation is not a main problem, because it is within the range of 10^{-5} - 10^{-3} [5]. Figures 14 and 15 show the characteristics of the Blackman apodized FBG reflectivity for L = constant = 8 mm.

It is clear that, Fig. 14 shows an increase in the maximum reflectivity, while Fig. 15 shows a decrease in the reduction of the sidelobes. This is a disadvantage of the increase of the index modulation maximum amplitude Δn. To interpret this phenomenon, the length now is kept constant (L = 8 mm). For $\Delta n = 0.3 \times 10^{-3}$, $\Delta n(z)$ will vary from

zero at z = 0 to 0.3 x 10^{-3} at z = (8 mm / 2)= 4 mm, while, for $\Delta n_N = 0.543 \times 10^{-3}$, $\Delta n(z)$ will vary from zero at z = 0 to 0.543×10^{-3} at z = (8 mm / 2) = 4 mm. Therefore, the gradual change of $\Delta n(z)$ is better for $\Delta n = 0.3 \times 10^{-3}$, Fig. 16.
Modifications can be applied to the Blackman apodized FBG, by the increase of its length, or, by the increase of its index modulation maximum amplitude, to increase its strength to the value of $(kL)_{cutoff}$, such that its reflectivity becomes 99%. Comparing Fig. 14 and Fig. 11, one notes that although both of them have the same strength, the bandwidth of the modified Blackman profile by the increase of length, is less than that of the modified by the increase of index modulation maximum amplitude.
To check this observation, one has to illustrate the general reflectivity behavior at constant strength with the change of length for the uniform FBG, Fig. 17. As expected, longer gratings produce narrower spectral linewidth.

One can conclude that, the Blackman profile is the best in the reduction of sidelobes. To increase its reflectivity, increasing the length is better than increasing the index modulation maximum amplitude, because it has the advantages of narrower linewidth and more reduction of the sidelobes.

C – Simultaneous change of the index modulation maximum amplitude and length of the AFBG

One goes in the direction of increasing the length and decreasing the index modulation maximum amplitude. The length may increase up to 100 mm, which is the maximum possible value [10]. The length is increased such that

$$\int_0^{L_N} k_N(z)dz = (kL)_{cutoff}, \tag{29}$$

$$k_N(z) = \frac{\eta\pi\Delta n_N(z)}{\lambda_B}, \tag{30}$$

Concerning the Blackman profile and substituting Eq.(30) into Eq.(29) using Eq. (21), one can get

$$\int_0^{L_N} \frac{\eta\pi}{\lambda_B}\left[\Delta n_N\left(\frac{1+1.19\cos(x)+0.19\cos(2x)}{2.38}\right)\right]dz = (kL)_{cutoff} = 3,$$

$$x = \frac{2\pi\left(z - \frac{L_N}{2}\right)}{L_N}. \tag{31}$$

This results in $\Delta n_N = 4.344 \times 10^{-5}$.
Similarly, Eq.(31) is solved for the other profiles giving the results presented in Table 4 .

Table 4 Comparison of different apodization profiles.

Apodization profile	New maximum amplitude of index modulation Δn_N
Raised sine	3.650×10^{-5}
Sine	2.867×10^{-5}
Sinc	3.096×10^{-5}
Gaussian	2.598×10^{-5}
Hamming	3.468×10^{-5}
tanh	2.208×10^{-5}
Barttlet	3.650×10^{-5}
Blackman	4.344×10^{-5}
Cauchy	2.592×10^{-5}

One must keep in mind that, the increase of the maximum amplitude of index modulation is not a main problem. It has a value in the range $10^{-5} - 10^{-3}$ [5]. Figures 18 and 19 show the reflectivity of the Blackman AFBG for $L_N = 100$ mm and $\Delta n_N = 4.344 \times 10^{-5}$.
It is concluded, from Figs. 18 and 19, that this design is the best for sidelobes reduction because it has the best gradual change in $\Delta n(z)$, Fig. 5.20, and also, it has the narrower bandwidth.

Now, one can safely increase the number of cascaded FBGs, decrease the guard band, Fig. 21 and increase the EDFL output wavelengths, Fig. 22 [4].
The channel wavelengths in a dense wavelength division multiplexing (DWDM) system are usually equally spaced in optical frequency based on the International Telecommunication Union (ITU) industrial standard. According to the ITU, the channel spacing is 100 GHz and the wavelengths are precisely selected [5]. This requires an increase in the cascaded FBGs such that their reflectivity is like that shown in Fig. 23. The laser output spectrum for the DWDM system is illustrated in Fig. 24.

4. Conclusion

In this work, a simple multi-wavelength laser using a CFBG, cascaded AFBGs and an EDF has been demonstrated. The CFBG has a reflection bandwidth of 13 nm centered about 1550 nm with a reflectivity of -3 dB. Cascaded FBGs are suggested to be apodized using the Blackman profile with maximum sidelobes reduction, narrower bandwidth, maximum reflectivity of 99% and length of 100 mm. For DWDM systems, 16-output lasings with wavelengths that coincide with the ITU industrial standard are generated with nearly constant total output power and constant 3-dB linewidth. This configuration can be used to generate any output lasings number with any other wavelengths by changing the number of the CAFBGs and the Bragg wavelengths of the CAFBGs, respectively.

5. References

[1] Xinhuan Feng, Lei Sun, Lingyun Xiong, Yange Liu, Shuzhong Yuan, Guiyun Kai and Xiaoyi Dong, "Swichable and tunable dual-wavelength erbium-doped fiber laser based on one fiber Bragg grating, " Optical Fiber Technol. , vol. 10, pp. 275–282, 2004.
[2] Zhao Chun-Liu, Yang Xiufeng, Lu Chao, Ng Jun Hong, Guo Xin, Partha Roy Chaudhuri and Dong Xinyong, "Switchable multi-wavelength erbium-doped fiber lasers by using cascaded fiber Bragg gratings written in high birefringence fiber, "Opt. Commun. , vol. 230, pp. 313–317, 2004.
[3] Qinghe Mao and John W. Y. Lit, "Switchable multi-wavelength erbium-doped fiber lasers with cascaded fiber cavities, "IEEE Photon. Technol. Lett., vol. 14, pp. 612–614, 2002.
[4] Shinji Yamashita, Muneo Yokooji, "Channel spacing-tunable sampled fiber Bragg grating by linear chirp and its application to multiwavelength fiber laser, " Opt. Commun. , Vol. 263, pp. 42–46, 2006.
[5] Andreas Othonos and Kyriacos Kalli, Fiber Bragg Gratings: Fundamentals and Applications in Telecommunications and Sensing, 2001.
[6] Johannes Skaar, Synthesis and characterization of fiber Bragg gratings, 2000.
[7] D.K.W Lam and B.K. Garside, "Characterization of single-mode optical fiber filters, "Appl. Opt., vol. 20, pp. 440–445, 1981.
[8] Dae Seung Moon, Un-Chul Paek and Youngjoo Chung, "Multi-wavelength linear-cavity tunable fiber laser using a chirped fiber Bragg grating and a few-mode fiber Bragg grating,"Opt. Express, vol. 13, pp. 5614–5620, 2005.
[9] Jianliang Yang, Swee Chuan Tjin and Nam Quoc Ngo, "Wideband tunable linear-cavity fiber laser source using strain-induced chirped fiber Bragg grating,"Opt. and Laser Technol., vol. 36, pp. 561–565, 2004.
[10] Karin Ennser, Mikhail N. Zervas and Richard I. Laming. "Optimization of apodized linearly chirped fiber gratings for optical communications,"IEEE Journal of Quantum Electronics, Vol.34, pp.770–778, 1998.
[11] Daniel Pastor, Jose Capmany, Diego Ortega and Javier Marti, "Design of apodized linearly chirped fiber gratings for dispersion compensation," J. Lightwave Technol., vol. 14, pp. 2581–2583, 1996.

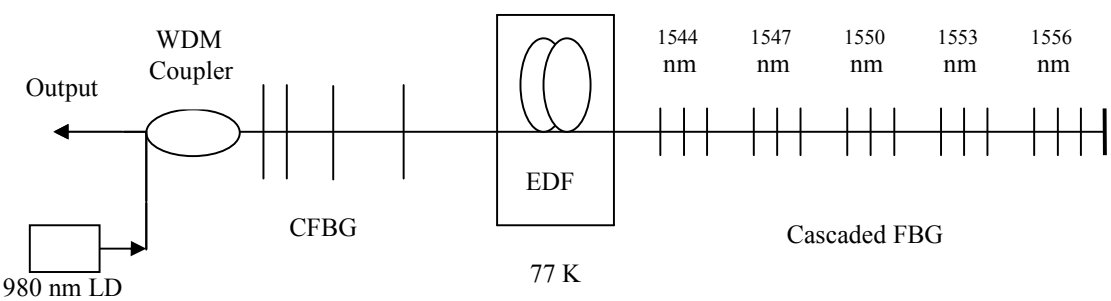

Figure 1 The schematic of multi-wavelength EDFL

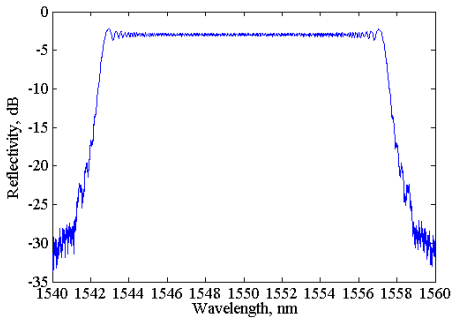

Figure 2 Reflection spectrum of the chirped fiber Bragg grating.

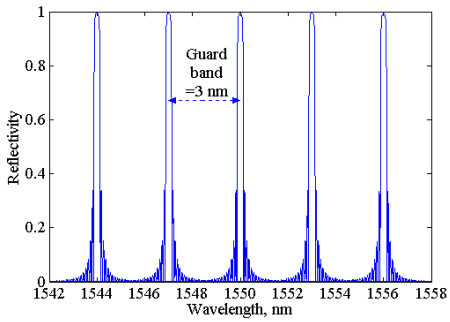

Figure 3 Reflection spectrum of the cascaded uniform FBGs.

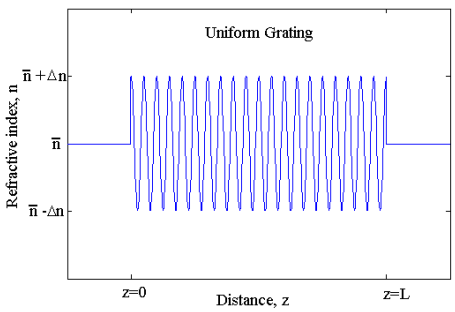

Figure 4 Refractive index profile of the uniform FBG.

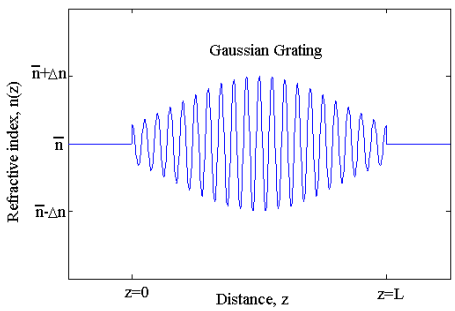

Figure 5 Refractive index profile of the Gaussian apodized FBG.

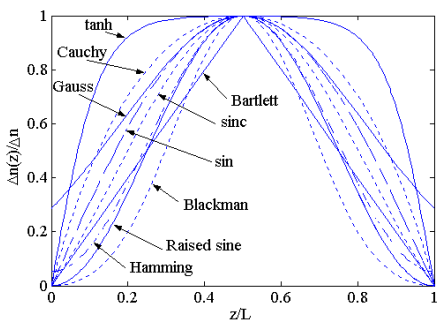

Figure 6 The various apodization profiles.

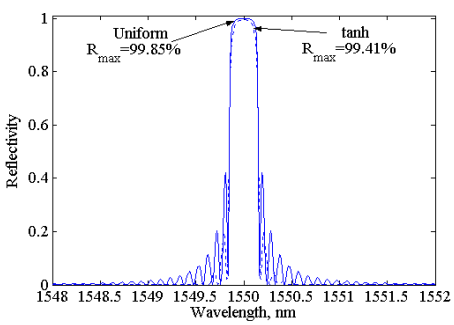

Figure 7-(a) Maximum reflectivity of the uniform FBG and tanh profile.

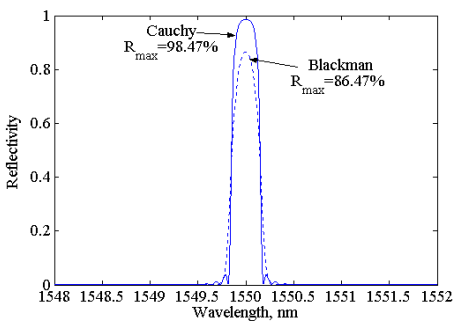

Figure 7-(b) Maximum reflectivity of the Cauchy and Blackman profiles.

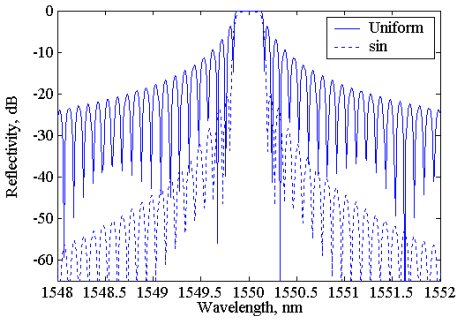

Figure 8-(a) Sidelobes reduction in the sine profile.

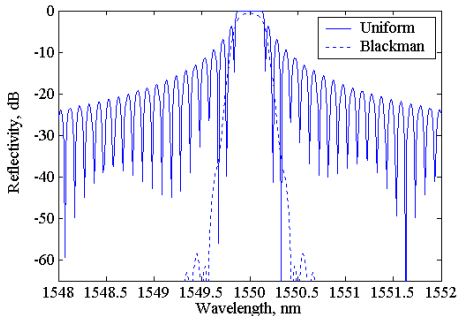

Figure 8-(b) Sidelobes reduction in the Blackman profile.

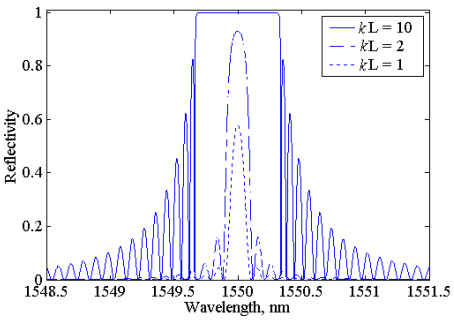

Figure 9 Reflection spectral response versus wavelength for a uniform FBG at different values of *k*L.

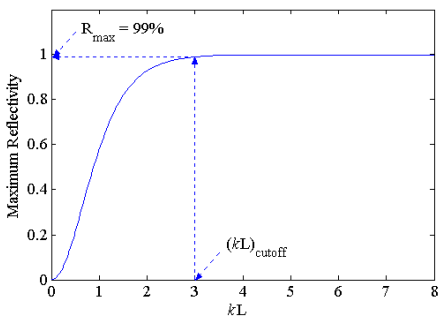

Figure 10 Maximum reflectivity versus (*k*L) at $\lambda = \lambda_B$.

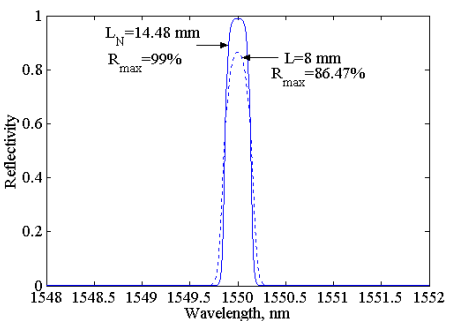

Figure 11 Reflectivity of Blackman profile at L_N =14.48 mm and at L = 8 mm.

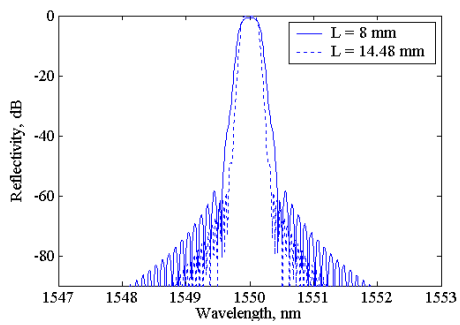

Figure 12 Reflectivity of Blackman profile at L =14.48 mm and at L = 8 mm showing the sidelobes.

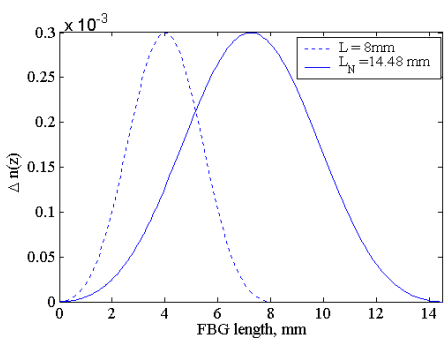

Figure 13 Change of Δn(z) for L = 8 mm and L_N = 14.48 mm when $\Delta n = 0.3 \times 10^{-3}$ = constant.

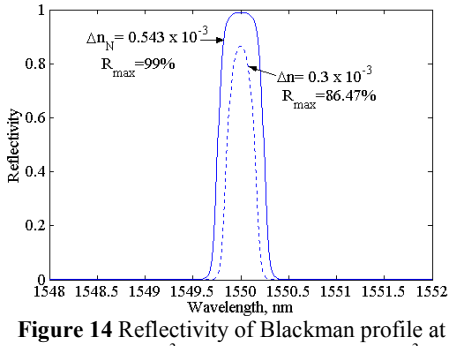

Figure 14 Reflectivity of Blackman profile at $\Delta n = 0.3 \times 10^{-3}$ and at $\Delta n_N = 0.543 \times 10^{-3}$.

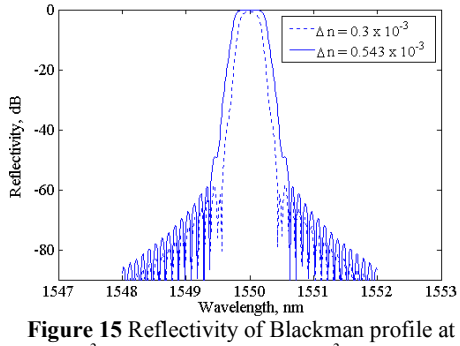

Figure 15 Reflectivity of Blackman profile at $\Delta n = 0.3 \times 10^{-3}$ and at $\Delta n_N = 0.543 \times 10^{-3}$ showing sidelobes.

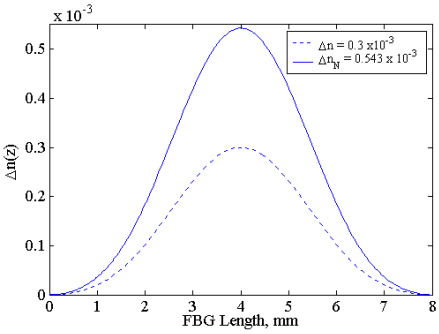

Figure 16 Change of $\Delta n(z)$ for $\Delta n = 0.3$ and $\Delta n_N = 0.543$ when L = constant = 8 mm.

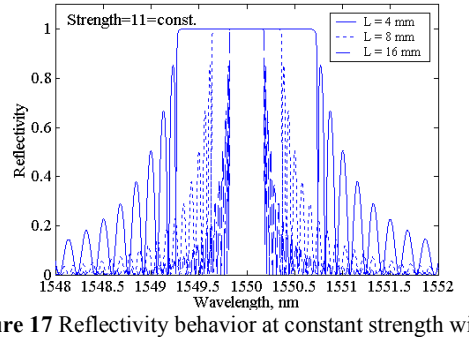

Figure 17 Reflectivity behavior at constant strength with L = 16, 8 and 4 mm.

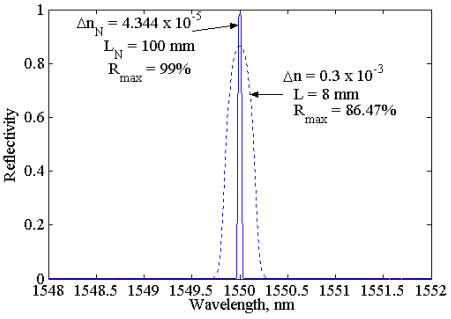

Figure 18 Reflectivity of Blackman profile showing maximum reflectivity.

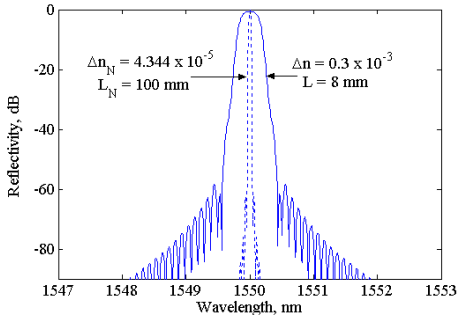

Figure 19 Reflectivity of Blackman profile showing sidelobes.

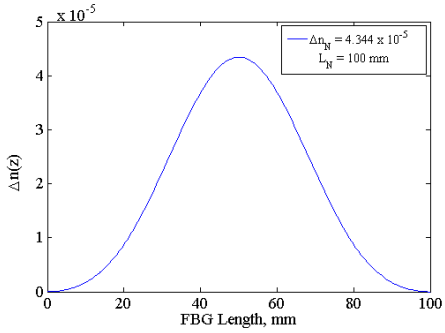

Figure 20 Change of $\Delta n(z)$ for $L_N = 100$ mm and $\Delta n_N = 4.344 \times 10^{-5}$.

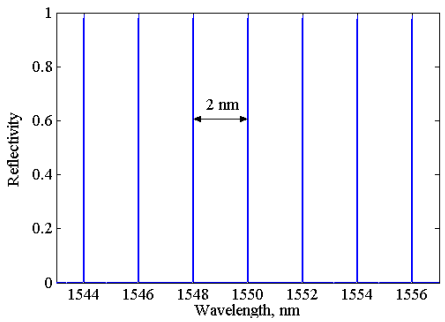

Figure 21 Reflection spectrum of the cascaded Blackman apodized FBGs.

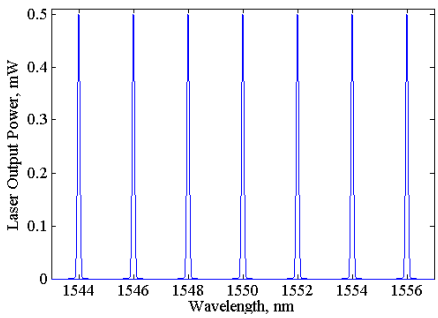

Figure 22 Optical spectra of multi-wavelength EDFL after apodization.

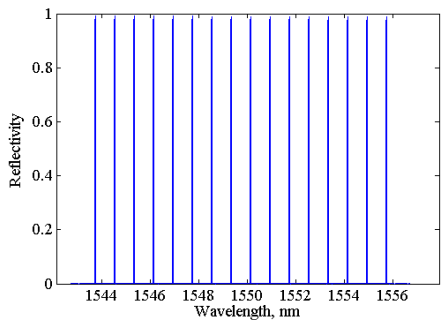

Figure 23 Reflection spectrum of the cascaded Blackman AFBGs for DWDM.

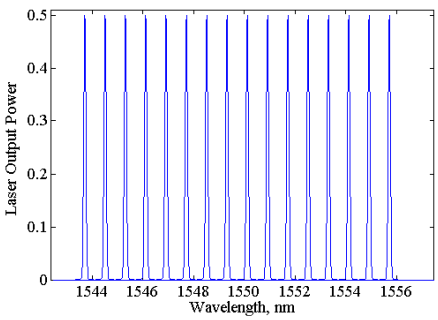

Figure 24 Optical spectra of multi-wavelength EDFL after apodization for DWDM.